PHYSICAL REVIEW C **76**, 064608 (2007)

Landau-Zener effect in fission

M. Mirea
Horia Hulubei National Institute for Physics and Nuclear Engineering, 077125 Bucharest, Romania

L. Tassan-Got, C. Stephan, and C. O. Bacri
Institute de Physique Nucleaire, F-91406 Orsay Cedex, France

R. C. Bobulescu
Faculty of Physics, P.O. Box MG-11, Bucharest, Romania

(Received 10 August 2007; revised manuscript received 15 October 2007; published 21 December 2007)

A model that takes into account the Landau-Zener promotion mechanism during fission was developed recently. The structures observed in the subthreshold neutron-induced fission of ^{232}Th are investigated employing this model. Theoretical single-particle excitations of a phenomenological two-humped barrier are determined by solving a system of coupled differential equations for the motion along the optimal fission path. A rather good agreement with experimental data is obtained using a small number of independent parameters. It is predicted that the structure at 1.4 and 1.6 MeV is mainly dominated by a spin 3/2 partial cross section with a small admixture of spin 1/2, while the structure at 1.7 MeV is given by a large partial cross section of spin 5/2.

DOI: 10.1103/PhysRevC.76.064608 PACS number(s): 24.75.+i, 21.60.Cs, 24.10.Eq, 25.70.Ef

I. INTRODUCTION

It is well known that the fission barrier in the actinide region exhibits a double humped shape. This double barrier, postulated in the frame of the microscopic-macroscopic model, provided a unified explanation of a great number of experimental results. At excitation energies below or close to the fission barrier top, the properties associated with the double hump shape are more pronounced than in other energy domains. A large number of intermediate resonances appear in the subthreshold and threshold regions. The energies fall exactly in the region of interest of the nuclear reactors, that is, thermal neutrons up to several MeV. These resonant peaks cannot be evaluated correctly in terms of actual models. Actually, for evaluation purposes, two ingredients are of major importance: the penetrability of a double barrier parameterized from experimental data and a good model for the nuclear level density. The cross section is proportional with the number of states calculated in the transient point or saddle point configuration following a hypothesis dating from 1939 [1]. Moreover, to reproduce the resonant structure of the cross section, many transition states are introduced by hand. The population of these transition states is considered to be unity. An imaginary potential is also introduced in a phenomenological way in the second well region to simulate better the widths of these resonances. The single-particle effects and the dynamics of the process are neglected, despite the fact that it has been believed for a long time that these quantities affect drastically all observations. Recently, we proposed a new formalism [2] to treat the resonant structure of the cross section, providing the possibility to follow each single-particle level from the initial state of the compound nucleus up to scission, to determine the barriers associated with each specialization energy to calculate dynamically the probability of penetrating each barrier or the population of each transition state. By using a similar treatment, the best agreement between theory and experiment [3] that can be found in the literature was obtained for the fine structure of cluster decay treated as superasymmetric fission.

The measured neutron-induced fission cross-section behavior of nuclei in the thorium region represented a challenge for nuclear physicists concerning the shape of the potential energy surface. The experimental data suggested the existence of a triple-humped barrier. The neutron-induced cross-sections of ^{230,232}Th exhibit multiple fine structures [4–6] superimposed on a gross structure of the threshold cross-section. If the fine structure is interpreted as a series of rotational states constructed on a β-vibrational state produced in some well of the deformation energy, it is straightforward to postulate the existence of a triple-humped barrier. The spacing between the members of the band is so small that it is consistent only with a prolate deformation that reaches the vicinity of the second-barrier top. The analysis of Ref. [4] indicates that an intermediate state nucleus must exist at a deformation considerably larger than that of the normal value. A ternary minimum obtained theoretically in the potential energy surface of ^{210}Po [7] made this hypothesis credible. Therefore, a shallow minimum was assumed at this deformation to create a new β-vibrational state. Angular distribution analysis [8,9] confirmed the existence of the triple well. Up to now, the assumption of a triple-humped barrier seems to be the best interpretation for the fine structure of intermediate cross-section resonances [10].

On the other hand, our analysis explores a different way to consider the cross-section resonant structure phenomenon by quantifying the dynamical single-particle effects associated with vibrational resonances produced in the second well [2]. Our exploratory investigation showed that the ^{230}Th neutron-induced fission threshold resonant structure can be explained [11] by rearrangements of single-particle orbitals on the way from the initial configuration of the compound nucleus up to scission. This resonant structure depends also on the dynamics of the process.

Section II provides a general description of the formalism intended for the evaluation of single-particle excitations, and results concerning the intermediate structure of the fission cross-section are extensively presented in Sec. III. Comments are made in Sec. IV.

II. SINGLE-PARTICLE EXCITATIONS

In most usual theoretical treatments of nuclear fission, the whole nuclear system is characterized by some collective coordinates associated with some degrees of freedom that determine approximately the behavior of many other intrinsic variables. The basic ingredient in such an analysis is a shape parametrization that depends on several macroscopic degrees of freedom. The generalized coordinates associated with these degrees of freedom vary in time leading to a split of the nuclear system in two separated fragments. A microscopic potential must be constructed to be consistent with this nuclear shape parametrization. It is known that a nuclear shape can be well characterized for fission processes if the following conditions are satisfied [12]: (i) The three most important degrees of freedom, that is, elongation, necking, and mass asymmetry, must be taken into account. (ii) A single sphere and two fragments should be allowed configurations. (iii) The flatness of the neck must be an independent variable. All these conditions are fulfilled in the following. By solving the Schrödinger equation for a reasonable mean field potential associated with the nuclear shape parametrization, the single-particle energies are determined. In the case of odd-nucleon systems, the potential barrier must be increased with an excitation associated with the unpaired nucleon. The amount by which the barrier is increased can be estimated within the specialization energy [13]. This quantity can be interpreted as the excess of the energy of the unpaired nucleon with a given spin over the energy of the same spin nucleon state of lowest energy.

In the present work, an axial-symmetric nuclear parametrization is obtained by smoothly joining two intersected spheres of different radii R_1 and R_2 with a neck surface generated by the rotation of a circle of radius R_3 around the symmetry axis, as displayed in Fig. 1. The surface equation is given in cylindrical coordinates:

$$\rho_s(z) = \begin{cases} \sqrt{R_1^2 - (z - z_1)^2}, & z \leqslant z_{c1} \\ \rho_3 - s\sqrt{R_3^2 - (z - z_3)^2}, & z_{c1} < z < z_{c2} \\ \sqrt{R_2^2 - (z - z_2)^2}, & z_{c2} \leqslant z, \end{cases} \quad (1)$$

where z_{c1} and z_{c2} define the region of the necking. The meaning of the geometrical symbols that depends on the shape parametrization can be understood by inspecting Fig. 1. This parametrization allows us to characterize a single nucleus or two separated nuclei. Throughout the paper, the subscripts 0, 1, and 2 indicate the parent, the heavy, and the light fragment, respectively. If $S = 1$, the shapes are necked in the median surface characterizing scission shapes and if $S = -1$ the shapes are swollen characterizing the ground state and saddle points. The macroscopic parameters used in the following are denoted $R = z_2 - z_1$ (elongation), $C = S/R_3$ (necking), and $\eta = R_1/R_2$ (mass asymmetry). For large distances between the two nascent fragments, the configuration given by two separated spheres is reached.

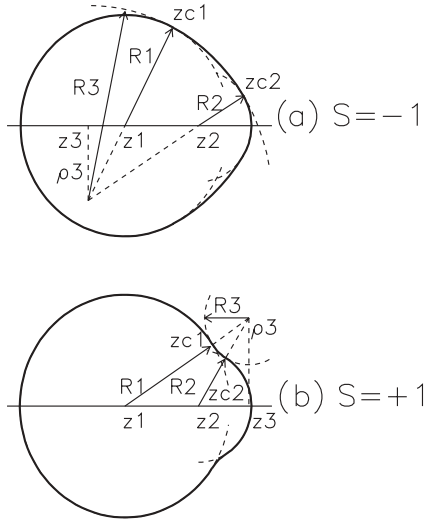

FIG. 1. Nuclear shape parametrization. z_1, z_2, and z_3 are the positions of the centers of circles of radii R_1, R_2 characterizing the two nascent fragments and of R_3 determining the neck, respectively. If $s = 1$, the shape is necked, otherwise the shape is swollen in the median surface. The distance between the two centers z_1 and z_2 determines the elongation R.

A way to obtain the sequence of nuclear shapes available for fission is to use the least action principle [14]. It is very difficult to treat the three independent generalized coordinates in the same time to minimize the action integral. Some simplifying assumptions must be introduced. As mentioned also in Ref. [15], microscopic approaches to fission [16,17] established that the second saddle point is asymmetrical with a value compatible with the observed mass ratio. In the same time, in the region of the second barrier, the mass-asymmetry component of the inertia tensor is very large [18]. So, the variations of the mass-asymmetry generalized coordinate are hindered in this region. Also, for elongations smaller than that of the outer barrier, the mass-asymmetry component of the inertia is much lower. Therefore, up to the second-barrier top, the mass-asymmetry coordinate can be modified without enhancing too much the value of the action integral. Moreover, even the deformation energy is less sensitive to variations of the mass-asymmetry coordinate in the region of compact shapes. As in Ref. [18], this observation allows us to reduce the number of parameters and to rend our problem tractable. Therefore, the evolution of the mass asymmetry generalized coordinate will be *a priori* fixed in the following. It is assumed that the ratio R_1/R_2 varies linearly from unity (first-barrier top) to the value associated with the final mass partition (second-barrier top). The mass asymmetry in the outer barrier region is deduced by considering that the volume occupied by the light fragment equals the final one.

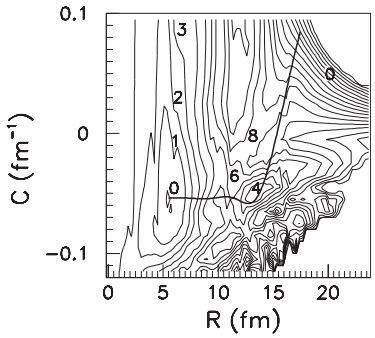

FIG. 2. Deformation energy in MeV for the partition $^{233}\mathrm{Th} \rightarrow {}^{98}\mathrm{Sr} + {}^{135}\mathrm{Te}$. C represents the curvature of the neck and R the distance between the centers of the fragments. Positive values of C characterize necked-in shapes. The mass asymmetry is varied linearly with R from a value $\eta(R \approx 5\,\mathrm{fm}) = 0$ (close to the ground state of the compound nucleus) to the final value $\eta = A_1/A_2$ (in the vicinity of the top of the second barrier). The step between two equipotential lines is 1 MeV. Several values of the deformation energy are marked on the plot. The dynamic trajectory is represented with a thick line that starts in the first well, penetrates the first barrier, attains the second well, and finally tunnels the second barrier toward scission.

The deformation energy of the nuclear system is the sum between the liquid drop energy and the shell effects, including pairing corrections. The macroscopic energy is obtained in the framework of the Yukawa-plus-exponential model extended for binary systems with different charge densities [19]. The Strutinsky prescriptions [20] were computed on the basis of the Superasymmetric Two Center Shell Model (STCSM) [21,22]. For one of the most probable partitions $^{233}\mathrm{Th} \rightarrow {}^{98}\mathrm{Sr} + {}^{135}\mathrm{Te}$, the deformation energy as a function of C and R is plotted in Fig. 2. The heavy fragment issued in this reaction is spherical, while the light one is little deformed, allowing a description in terms of our nuclear shape parametrization.

The theoretical study of binary disintegration processes is limited by the difficulties encountered in the calculation of single-particle levels for very deformed one-center potentials. On one hand, central oscillator potentials are not able to describe in a correct manner the shapes for the passage of one nucleus to two separated nuclei without including a large number of multipole deformation parameters, and, on the other hand, for very large prolate deformations the sum of single-particle energies reaches an infinite value, as evidenced within the deformed oscillator model. These difficulties are surpassed by considering that the mean field is generated by nucleons moving in a double center potential. This kind of model allows us to describe scission configurations within a small number of degrees of freedom. A more realistic version of the two-center shell model was realized recently [22] and it is used to generate the single-particle energy evolutions from the ground state up to the formation of two separated fragments.

The shape of the fission barrier can be obtained if the trajectory of the nuclear system in our three-dimensional configuration space is known. This trajectory emerges by minimizing numerically the action functional that gives the quantum penetrability

$$P = \exp\left\{-\frac{2}{\hbar}\int_{R_i}^{R_f} \times \sqrt{2V(R,C,\eta)M\left(R,C,\eta,\frac{\partial C}{\partial R},\frac{\partial \eta}{\partial R}\right)}dR\right\} \quad (2)$$

in the semiclassical Wentzel-Kramers-Brillouin approximation [20]. The two turning points R_i and R_f denote the elongations that characterize the first well and the exit point of the barrier, respectively. Here $V(R, C, \eta)$ is the deformation energy and $M(R, C, \eta, \frac{\partial C}{\partial R}, \frac{\partial \eta}{\partial R})$ is the effective mass along the trajectory. The inertia is computed in the frame of the Werner-Wheeler approximation [23], that means the flow of the fluid is idealized as nonrotational, nonviscous, and hydrodynamic. Using the minimal action principle, in general, the nuclear system does not follow a path characterized by minimal values of the deformation energy, so that the trajectory does not interpolate barrier saddle point values.

Having in mind the assumption imposed for the variation of the mass asymmetry, the action integral must be minimized in a two-dimensional space spanned by C and R. The first turning point R_i is fixed but the second R_f lies on the equipotential line that characterizes the exit from the outer barrier; that is, R_f is a function of C. A simple numerical method is used to find the paths characterized by different values of R_f, associated with local minimums. For that purpose, the function $C = f(R)$ is approximated with a spline function of n variables C_j $(j = 1, n)$ in fixed mesh points R_j located in the interval $[R_i, R_f]$ along the elongation axis. A numerical expression for the WKB functional (2) that depends only on the parameters C_j is obtained. This expression is minimized numerically. For every value of R_f a local minimum is obtained. The best values are retained. The trajectory is displayed on Fig. 2. This dynamical trajectory starts from the ground state, reaches the region of the second well, and the slope changes suddenly to penetrate the outer barrier. Between the first and second well, the macroscopic coordinate C is less than 0; that is, the shapes are swollen in the median region. Penetrating the second well, the shapes become necked. The theoretical potential barrier obtained along the minimal action path is plotted in Fig. 3. The height of the outer barrier is very large; therefore, some corrections are required to obtain realistic values of the fission cross-section. This is the main reason that leads to use a phenomenological barrier in calculating the cross-section. The

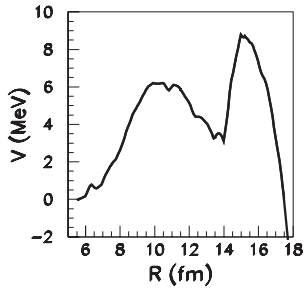

FIG. 3. Theoretical dynamical barrier calculated along the minimal action trajectory as function of the elongation R.

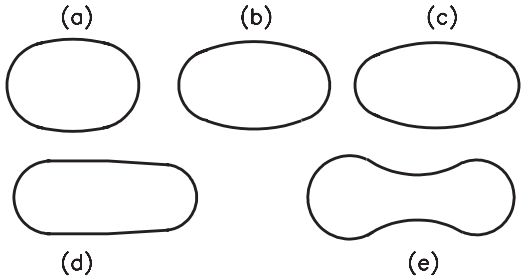

FIG. 4. The shapes obtained along the minimal action trajectory. (a) The ground state with elongation $R = 5.8$ fm and necking coordinate $C = -0.053$ fm^{-1}. (b) The region of the first barrier with $R = 10.57$ fm and $C = -0.04$ fm^{-1}. (c) The region of the second well with $R = 13.69$ fm and $C = -0.0508$ fm^{-1}. (d) The region of the second barrier with $R = 15.139$ fm and $C = -0.008$ fm^{-1}. (e) The region of the exit from the barrier with $R = 17$ fm and $C = 0.085$ fm^{-1}.

first well is located at approximately $R = 5.5$ fm and identifies the fundamental state. In Fig. 4, the nuclear shapes of the extreme values of the barrier are displayed. Concerning the parameters of the double barrier, a recent contribution devoted to this subject [24] showed that actual models cannot approach yet the experimental determined values to reproduce at least qualitatively the cross-section. This motivated us in the use of a phenomenological barrier to have decent values of the cross-section.

At this point, some discussions are imposed. In Ref. [17] five degrees of liberty were used to characterize the shape. The minimization was realized in a static way, the inertia being neglected. It is possible that the results change if a minimization of the action integral will be performed. In the frame of the referenced calculations, a small dent was obtained in the median region of the shape for the saddle point configuration of the outer barrier. From a theoretical point of view, such a dent will lead to only a single channel in the final distribution of fission products. This aspect contradicts the random neck rupture theory [12]. On another hand, our model can be criticized because the dynamical minimization was done only in a two-dimensional space. But, the works published up to now concerning action integral minimization are realized also in a two-dimensional configuration space, while the potential is minimized statically at each point for other coordinates as in Ref. [25], for example. The procedure used in Ref. [25], in conjunction with the zig-zag linear path implied by their minimization recipe, represents a peculiar behavior because the dependence of the inertia as a function of the coordinates is unclear. Another aspect that can be criticized in our work is the use of a macroscopic model for the effective mass. The cranking model supplies mass parameters six or seven times larger. However, if the hydrodynamical mass parameters are multiplied by a factor of 6 or 7, the minimization procedure will give the same least action path. The single difference is that the value of the action integral, which is obsolete in our context, will be changed. Without entering in details, the Werner-Wheeler approximation gives the main trends for the variations of the effective mass parameters as the microscopic models. As a

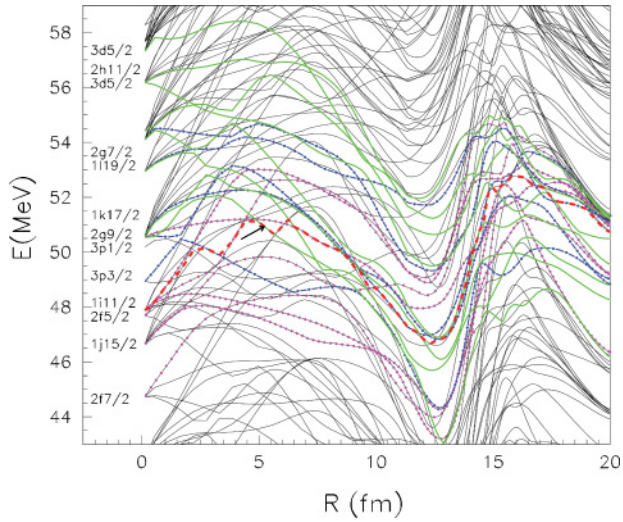

FIG. 5. (Color online) Neutron level scheme as a function of the elongation. At elongation zero, the shape parametrization gives a spherical nucleus and the spectroscopic notations are available. For low values of the deformations, the system behaves as a Nilsson level scheme. Asymptotically ($R \to \infty$) the two diagrams of the two formed fragments are superimposed. In the adiabatic representation, the Fermi level is displayed with a thick dashed line (red). The eight selected levels with $\Omega = 1/2$ are represented with a full thick line (green), the five levels with $\Omega = 3/2$ are plotted with dot-dashed thick lines (blue), the four times $\Omega = 5/2$ and three times 7/2 levels are marked with dotted lines (violet, smaller distance between points for $\Omega = 5/2$). The ground state of the compound nucleus is indicated with an arrow.

result of the minimization, the dynamical trajectory deviates from the adiabatic one in such a way that abrupt variations of the generalized coordinates are not allowed. Abrupt variations produce large values of the generalized coordinate derivatives that enter in the formula of the effective mass along the trajectory and the inertia increases. The main effect is that the trajectory becomes smoother and the barrier increases. Surprisingly or not, our trajectory resembles with that given in Ref. [26] where cranking parameters were used.

Using the STCSM the neutron diagram is computed along the minimal action trajectory, as displayed in Fig. 5. Up to $R \approx 5.5$ fm the nuclear system is considered reflection symmetric. From the first well up to scission, the system loses the reflection symmetry to reach the final partition $^{233}\mathrm{Th} \to {}^{98}\mathrm{Sr} + {}^{135}\mathrm{Te}$. In these circumstances, the parity is no longer a good quantum number. So, the levels are characterized only by the spin projection Ω as good quantum numbers. The Nilsson coefficients [27] of the orbital momentum operators ($\kappa = 0.063$ and $\eta = 0.8$) were determined to reproduce as best as possible the experimental sequence of the first excited levels in ^{233}Th. The first single-particle excited states are retrieved: an $\frac{1}{2}^+$ state (fundamental level) emerging from $2g_{9/2}$ followed by a $\frac{5}{2}^+$ one.

To determine the cross-section, several single-particle levels are selected that lie as close as possible to the Fermi energy region. These levels give the major contribution in the strength of the fission channel due to their low excitation energy and

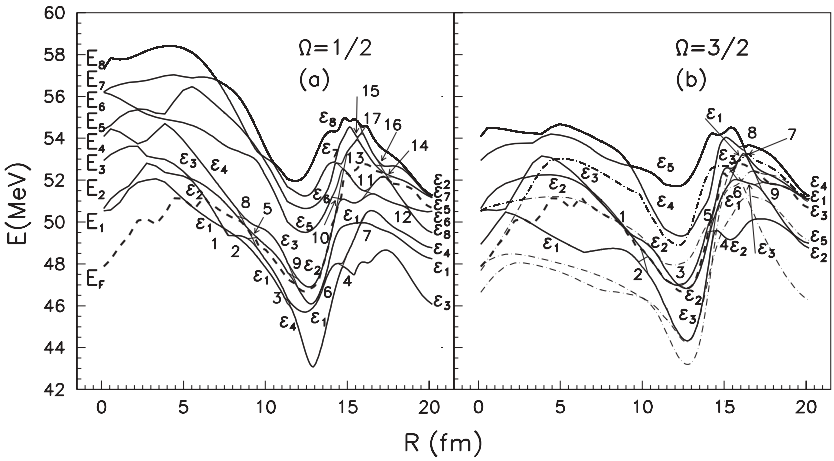

FIG. 6. (a) The eight selected levels with $\Omega = 1/2$. The Fermi level in the adiabatic representation is denoted E_F and is represented with a dashed line. The avoided level crossing regions are numbered and the diabatic levels ϵ_i identified. In the ground state configuration, the ϵ_1 level (emerging from E_1) is superimposed on E_F. At $R \approx 20$ fm, E_F is located between ϵ_6 and ϵ_5, while the adiabatic level emerging from E_1 dropped to ϵ_3. (b) As in plot (a) for the five levels with $\Omega = 3/2$. With thin dot-dashed lines the four $\Omega = 5/2$ adiabatic levels are also displayed.

the large amount of macroscopic kinetic energy available for disintegration. Concerning the $\Omega = 1/2$ workspace, eight selected levels, E_1 up E_8, are extracted separately in the left panel of Fig. 6 as an example. The Fermi level is denoted E_F. The diabatic levels of the subspace $\Omega = 3/2$ are displayed in the right panel of the same figure. In the following, for simplicity, the discussion is restricted only for the subspace $\Omega = \frac{1}{2}$. For $\Omega = \frac{3}{2}, \frac{5}{2}, \frac{7}{2}$, the same procedure as in the case of $\Omega = \frac{1}{2}$ is used.

A first behavior can be noticed. The nucleon located on the adiabatic level emerging from E_1 reaches a very unfavorable energy configuration after the scission. In the fundamental state, this unpaired nucleon is located on the fundamental level but arrives, in the adiabatic representation, at several MeV under the Fermi level (the ϵ_3 diabatic level). So, if the nucleon is initially on the ground state, it must follow a diabatic energy path to arrive in a more favorable energy configuration, that is, close to the last occupied level (in one of the diabatic states $\epsilon_6, \epsilon_5, \epsilon_7$, or ϵ_2). So, adiabatically, the fission strength for states with spin 1/2 is not favored. This effect is a direct consequence of the rearrangement of low spin orbitals during the disintegration. The number of levels with $\Omega = \frac{1}{2}$ in the two nascent fragments that are under the energy of the last occupied level is always larger than the same number in the compound nucleus. So, $\Omega = 1/2$ orbitals of the parent must decrease in energy to fill the levels located under the Fermi energy of the two fragments. This aspect somewhat hinders the possibility to fission through $\Omega = \frac{1}{2}$ channels. The next step is to study the energy paths followed by the unpaired nucleon in the single-particle diagram.

The realistic two-center diagram presented before provides an instrument to study the role of individual orbitals during the disintegration process in a way similar to the study of nucleus-nucleus collisions [28–31] or the α and cluster decays [32,33]. Levels with the same quantum numbers associated with some symmetries of the system cannot cross during the disintegration process and exhibit avoided level crossing. In our case, due to the axial symmetry of the system, the good quantum numbers are the projection of the spin Ω. The point of nearest approach between two levels of the same Ω defines an avoided level crossing region. If the internuclear distance varies, the transition probability of a nucleon between two adiabatic levels is strongly enhanced in the avoided level crossing region. This promotion mechanism is generically called the Landau-Zener effect.

Concerning the eight single-particle adiabatic levels $(E_1, \ldots, E_8)$ belonging to the $\Omega = 1/2$ workspace, the first step is to find the avoided level crossing regions. The avoided crossing regions can be obtained by plotting the energy differences between these adiabatic levels as in Fig. 7. Each pertinent avoided crossing is identified and numbered. The avoided crossings that have a chance to be located along the diabatic single-particle energy paths emerging from the

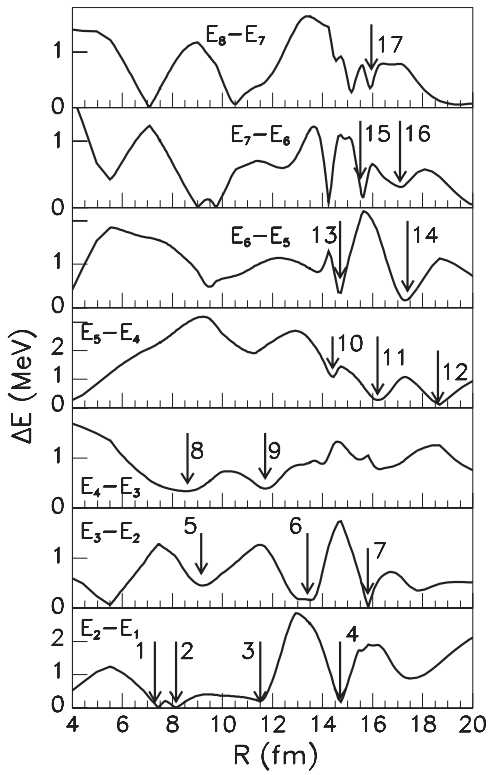

FIG. 7. Differences between the selected adiabatic levels. The avoided level crossing regions that appear between the adiabatic energies emerging from the initial states $E_1, \ldots E_4$ are numbered as in Fig. 6.

lower levels E_1, E_2, and E_3 are considered pertinent. Due to their low initial excitation energy, the transitions through these levels carry the major part of the fission strength. That property allows us to restrict our calculations only for an initial condition in which the occupation probability of one of these levels is one. The next step is to determine the probability of realization of each diabatic energy path emerging from these three levels. Concerning the $\Omega = 3/2$ subspace, the analysis is realized in the same manner for initial conditions restricted to the first three low energy levels.

Assuming an n-state approximation, the wave function of the unpaired nucleon can be formally expanded [34] in a basis of n diabatic wave functions $\phi_i(r, R)$ as

$$\Psi(r, R, t) = \sum_i^n c_i(t)\phi_i(r, R) \exp\left(-\frac{i}{\hbar}\int_0^t \epsilon_{ii} dt\right), \quad (3)$$

where the matrix elements with the diabatic states ϕ are abbreviated as

$$\epsilon_{ij} = \langle\phi_i|H|\phi_j\rangle, \quad (4)$$

where H is the STCSM Hamiltonian and c_i are amplitudes. Inserting Ψ in the time-dependent Schrödinger equation

$$\langle\phi_i|H - i\hbar\frac{\partial}{\partial t}|\Psi\rangle = 0, \quad (5)$$

the following system of coupled equations is obtained:

$$\dot{c}_i = \frac{1}{i\hbar}\sum_{j\neq i}^n c_j\epsilon_{ij} \exp\left(-\frac{i}{\hbar}\int_0^t (\epsilon_{jj} - \epsilon_{ii})dt\right). \quad (6)$$

To solve this system, the internuclear velocity $\dot{R}$, the diabatic energies, and the interaction matrix elements must be known. Excepting the relative velocity, the other ingredients are supplied by the STCSM. The diabatic states are constructed by using spline interpolations in the level crossing regions. The interaction matrix elements ϵ_{ij} between the diabatic states are a measure of the difference between adiabatic and diabatic energies. The occupation probability of each adiabatic level as function of R is now obtained by $p_{\epsilon_i} = |c_i|^2$. For the unpaired neutron initially located in the fundamental state E_1, the system (6) is solved within the boundary condition $c_1 = 1$ and $c_i = 0$ for $i \neq 1$. The occupation probabilities of each diabatic level plotted in Fig. 6 are represented in Fig. 8. Within the selected levels and avoided level crossings, 40 different energy paths of the unpaired neutron can be obtained as indicated in Table I. Here, an approximation is made by considering that the points of the avoided level crossings 1 and 2 form a single avoided level region. Otherwise, the number of paths gets doubled. Each path represents an excitation of the nuclear system. The probability of each path can be estimated. For example, it can be deduced from Fig. 8 that the path $\epsilon_1 - 2 - \epsilon_1 - 3 - \epsilon_4$ carries about 0.5 of the probability. The line between letters and digits connects diabatic levels and avoided level crossing regions. A strong mixing is produced in the region 4, which leads us to conclude that the paths $\epsilon_1 - 2 - \epsilon_1 - 3 - \epsilon_4 - 4 - \epsilon_3$ (No. 1 in Table I) and $\epsilon_1 - 2 - \epsilon_1 - 3 - \epsilon_4 - 4 - \epsilon_4 - 7$ each carry about 0.25 probability. Finally, it can be considered that the path $\epsilon_1 - 2 - \epsilon_1 - 3 - \epsilon_4 - 4 - \epsilon_4 - 7 - \epsilon_1$ (No. 2)

TABLE I. Energy paths open for the first $E_1\Omega = 1/2$ level.

No.	Energy path
1	$\epsilon_1 - 2 - \epsilon_1 - 3 - \epsilon_4 - 4 - \epsilon_3$
2	$\epsilon_1 - 2 - \epsilon_1 - 3 - \epsilon_4 - 4 - \epsilon_4 - 7 - \epsilon_1$
3	$\epsilon_1 - 2 - \epsilon_1 - 3 - \epsilon_4 - 4 - \epsilon_4 - 7 - \epsilon_4$
4	$\epsilon_1 - 2 - \epsilon_1 - 3 - \epsilon_1 - 6 - \epsilon_3 - 4 - \epsilon_3$
5	$\epsilon_1 - 2 - \epsilon_1 - 3 - \epsilon_1 - 6 - \epsilon_3 - 4 - \epsilon_4 - 7 - \epsilon_1$
6	$\epsilon_1 - 2 - \epsilon_1 - 3 - \epsilon_1 - 6 - \epsilon_3 - 4 - \epsilon_4 - 7 - \epsilon_4$
7	$\epsilon_1 - 2 - \epsilon_1 - 3 - \epsilon_1 - 6 - \epsilon_1 - 7 - \epsilon_1$
8	$\epsilon_1 - 2 - \epsilon_1 - 3 - \epsilon_1 - 6 - \epsilon_1 - 7 - \epsilon_4$
9	$\epsilon_1 - 2 - \epsilon_2 - 5 - \epsilon_2 - 9 - \epsilon_3 - 6 - \epsilon_3 - 4 - \epsilon_3$
10	$\epsilon_1 - 2 - \epsilon_2 - 5 - \epsilon_2 - 9 - \epsilon_3 - 6 - \epsilon_3 - 4 - \epsilon_4 - 8 - \epsilon_1$
11	$\epsilon_1 - 2 - \epsilon_2 - 5 - \epsilon_2 - 9 - \epsilon_3 - 6 - \epsilon_3 - 4 - \epsilon_4 - 8 - \epsilon_4$
12	$\epsilon_1 - 2 - \epsilon_2 - 5 - \epsilon_2 - 9 - \epsilon_3 - 6 - \epsilon_1 - 8 - \epsilon_1$
13	$\epsilon_1 - 2 - \epsilon_2 - 5 - \epsilon_2 - 9 - \epsilon_3 - 6 - \epsilon_1 - 8 - \epsilon_4$
14	$\epsilon_1 - 2 - \epsilon_2 - 5 - \epsilon_4 - 3 - \epsilon_4 - 4 - \epsilon_3$
15	$\epsilon_1 - 2 - \epsilon_2 - 5 - \epsilon_4 - 3 - \epsilon_4 - 4 - \epsilon_4 - 8 - \epsilon_1$
16	$\epsilon_1 - 2 - \epsilon_2 - 5 - \epsilon_4 - 3 - \epsilon_4 - 4 - \epsilon_4 - 8 - \epsilon_4$
17	$\epsilon_1 - 2 - \epsilon_2 - 5 - \epsilon_4 - 3 - \epsilon_1 - 6 - \epsilon_3 - 4 - \epsilon_3$
18	$\epsilon_1 - 2 - \epsilon_2 - 5 - \epsilon_4 - 3 - \epsilon_1 - 6 - \epsilon_3 - 4 - \epsilon_4 - 8 - \epsilon_1$
19	$\epsilon_1 - 2 - \epsilon_2 - 5 - \epsilon_4 - 3 - \epsilon_1 - 6 - \epsilon_3 - 4 - \epsilon_4 - 8 - \epsilon_4$
20	$\epsilon_1 - 2 - \epsilon_2 - 5 - \epsilon_4 - 3 - \epsilon_1 - 6 - \epsilon_1 - 7 - \epsilon_1$
21	$\epsilon_1 - 2 - \epsilon_2 - 5 - \epsilon_4 - 3 - \epsilon_1 - 6 - \epsilon_1 - 7 - \epsilon_4$
22	$\epsilon_1 - 2 - \epsilon_2 - 5 - \epsilon_2 - 9 - \epsilon_2 - 10 - \epsilon_5 - 11 - \epsilon_6 - 12 - \epsilon_8$
23	$\epsilon_1 - 2 - \epsilon_2 - 5 - \epsilon_2 - 9 - \epsilon_2 - 10 - \epsilon_5 - 11 - \epsilon_6 - 12 - \epsilon_6$
24	$\epsilon_1 - 2 - \epsilon_2 - 5 - \epsilon_2 - 9 - \epsilon_2 - 10 - \epsilon_5 - 11 - \epsilon_5 - 14 - \epsilon_8 - 12 - \epsilon_8$
25	$\epsilon_1 - 2 - \epsilon_2 - 5 - \epsilon_2 - 9 - \epsilon_2 - 10 - \epsilon_5 - 11 - \epsilon_5 - 14 - \epsilon_8 - 12 - \epsilon_6$
26	$\epsilon_1 - 2 - \epsilon_2 - 5 - \epsilon_2 - 9 - \epsilon_2 - 10 - \epsilon_5 - 11 - \epsilon_5 - 14 - \epsilon_5$
27	$\epsilon_1 - 2 - \epsilon_2 - 5 - \epsilon_2 - 9 - \epsilon_2 - 10 - \epsilon_2 - 13 - \epsilon_6 - 11 - \epsilon_6 - 12 - \epsilon_8$
28	$\epsilon_1 - 2 - \epsilon_2 - 5 - \epsilon_2 - 9 - \epsilon_2 - 10 - \epsilon_2 - 13 - \epsilon_6 - 11 - \epsilon_6 - 12 - \epsilon_6$
29	$\epsilon_1 - 2 - \epsilon_2 - 5 - \epsilon_2 - 9 - \epsilon_2 - 10 - \epsilon_2 - 13 - \epsilon_6 - 11 - \epsilon_5 - 14 - \epsilon_8 - 12 - \epsilon_8$
30	$\epsilon_1 - 2 - \epsilon_2 - 5 - \epsilon_2 - 9 - \epsilon_2 - 10 - \epsilon_2 - 13 - \epsilon_6 - 11 - \epsilon_5 - 14 - \epsilon_8 - 12 - \epsilon_6$
31	$\epsilon_1 - 2 - \epsilon_2 - 5 - \epsilon_2 - 9 - \epsilon_2 - 10 - \epsilon_2 - 13 - \epsilon_6 - 11 - \epsilon_5 - 14 - \epsilon_5$
32	$\epsilon_1 - 2 - \epsilon_2 - 5 - \epsilon_2 - 9 - \epsilon_2 - 10 - \epsilon_2 - 13 - \epsilon_2 - 15 - \epsilon_7 - 16 - \epsilon_8 - 14 - \epsilon_8 - 12 - \epsilon_8$
33	$\epsilon_1 - 2 - \epsilon_2 - 5 - \epsilon_2 - 9 - \epsilon_2 - 10 - \epsilon_2 - 13 - \epsilon_2 - 15 - \epsilon_7 - 16 - \epsilon_8 - 14 - \epsilon_8 - 12 - \epsilon_6$
34	$\epsilon_1 - 2 - \epsilon_2 - 5 - \epsilon_2 - 9 - \epsilon_2 - 10 - \epsilon_2 - 13 - \epsilon_2 - 15 - \epsilon_7 - 16 - \epsilon_8 - 14 - \epsilon_5$
35	$\epsilon_1 - 2 - \epsilon_2 - 5 - \epsilon_2 - 9 - \epsilon_2 - 10 - \epsilon_2 - 13 - \epsilon_2 - 15 - \epsilon_7 - 16 - \epsilon_7$
36	$\epsilon_1 - 2 - \epsilon_2 - 5 - \epsilon_2 - 9 - \epsilon_2 - 10 - \epsilon_2 - 13 - \epsilon_2 - 15 - \epsilon_2 - 17 - \epsilon_8 - 16 - \epsilon_8 - 14 - \epsilon_8 - 12 - \epsilon_8$
37	$\epsilon_1 - 2 - \epsilon_2 - 5 - \epsilon_2 - 9 - \epsilon_2 - 10 - \epsilon_2 - 13 - \epsilon_2 - 15 - \epsilon_2 - 17 - \epsilon_8 - 16 - \epsilon_8 - 14 - \epsilon_8 - 12 - \epsilon_6$
38	$\epsilon_1 - 2 - \epsilon_2 - 5 - \epsilon_2 - 9 - \epsilon_2 - 10 - \epsilon_2 - 13 - \epsilon_2 - 15 - \epsilon_2 - 17 - \epsilon_8 - 16 - \epsilon_8 - 14 - \epsilon_5$
39	$\epsilon_1 - 2 - \epsilon_2 - 5 - \epsilon_2 - 9 - \epsilon_2 - 10 - \epsilon_2 - 13 - \epsilon_2 - 15 - \epsilon_2 - 17 - \epsilon_8 - 16 - \epsilon_7$
40	$\epsilon_1 - 2 - \epsilon_2 - 5 - \epsilon_2 - 9 - \epsilon_2 - 10 - \epsilon_2 - 13 - \epsilon_2 - 15 - \epsilon_2 - 17 - \epsilon_2$

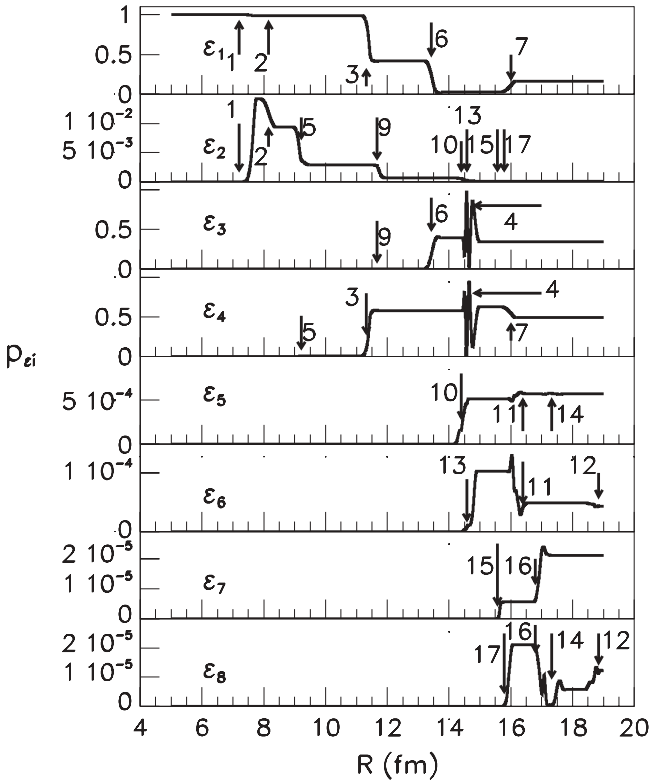

FIG. 8. The occupation probabilities of the diabatic levels $\epsilon_1, \ldots \epsilon_8$ as a function of the distance between the centers of the fragments. The same numbers as in Fig. 7 are used to identify the avoided level crossing regions. The internuclear velocity is 3.5×10^4 m/s, which leads to a reasonable reaction time (time to penetrate the barrier) of approximately 5×10^{-19} s. This example is constructed for an initial condition $p_{\epsilon_1} = 1$, while $p_{\epsilon_i} = 0 (i \neq 1)$. The occupation probabilities vary in the avoided level crossing regions.

has about 0.05 probability of realization while $\epsilon_1 - 2 - \epsilon_1 - 3 - \epsilon_4 - 4 - \epsilon_4 - 7 - \epsilon_4$ (No. 3) remains with 0.2. The other probabilities are estimated in the same manner. The same procedure is repeated for the case where the unpaired nucleon is initially located on the other selected levels.

The excitations of the barriers due to one diabatic path k is given by the specialization energy. Considering that the fundamental barrier corresponds to the nucleon at the Fermi energy, the excitation E_{xk} as function of R is

$$E_{xk}(R) = \sqrt{(\epsilon_k(R) - \lambda(R))^2 + \Delta^2(R)} - \Delta(R) \tag{7}$$

in the frame of the superfluid model. Here, ϵ_k is the single-particle energy of the path k, λ is the Fermi energy, and Δ is the gap. These excitations are added to the fundamental barrier. These quantities have the same meaning as the so-called transition bandheads found in the literature.

It is implicitly assumed that the excitations of the potential barrier are given only by the specialization energy and that the fundamental barrier is the same for all channels. The validity of the model can be checked by calculating also the dissipation during the tunneling of the barrier in the case of different channels. Variations of single-particle densities ρ_i can be evaluated by solving the next system of coupled equations as in Ref [18]:

$$\begin{aligned} i\hbar\dot{\rho}_i &= \kappa_i \Delta^* - \kappa_i^* \Delta \\ i\hbar\dot{\kappa}_i &= (2\rho_i - 1)\Delta - 2\kappa_i(\epsilon_i - \lambda), \end{aligned} \tag{8}$$

where $\rho_i = |v_i|^2$ and $\kappa_i = u_i^* v_i$, $\Delta = G \sum_i \kappa_i$. u_i and v_i are the complex BCS occupation and vacancy amplitudes. Equations (8) are generically known as the time-dependent Hartree-Fock-Bogoliubov (TDHFB) equations [35,36]. As mentioned in Ref. [36], a connection with the Landau-Zener effect is included in these equations. Levels undergo Landau-Zener transitions on virtual levels with coupling strengths given by the gap Δ. The difference between the total energy value E obtained within the TDHFB equations and E_0 given by the static BCS equations represents an approximation for the dissipation E_D:

$$E_D = E - E_0. \tag{9}$$

E is expressed simply in terms of ρ_i and κ_i,

$$E = 2\sum_i \epsilon_i \rho_i - G\left|\sum_i \kappa_i\right|^2 - G\sum_i \rho_i^2. \tag{10}$$

E_0 corresponds to ρ_i^0 and κ_i^0 associated with the lower energy state.

III. CROSS-SECTION

The partial fission cross section σ_f for a spin J of the compound nucleus and excitation energy E^* is obtained within a statistical principle:

$$\sigma_f(J, E^*) = \sigma_c(J, E^*)\frac{\Gamma_f(J, E^*)}{\Gamma_n(J, E^*) + \Gamma_\gamma(J, E^*) + \Gamma_{fT}(J, E^*)}, \tag{11}$$

where the ratio on the right-hand side is the probability that the system decays through fission. It is given by a ratio between energy widths for fission (subscript f), neutron emission (subscript n), and γ deexcitation (subscript γ). The subscript T addresses the total transmission in the fission channel including absorption in the second well. The neutron transmission was computed for a squared complex potential [37] to evaluate the compound nucleus cross section. To determine the participation of different Ω excitations in the fission channel for a given spin J of the compound nucleus, an unfolding procedure in terms of Clebsh-Gordon coefficients is used,

$$\Gamma_f(J, E^*) = \frac{1}{2\pi\rho(J, E^*, A)}\sum_{L=0}^{L_M}\sum_{\Omega}\frac{\langle JL\Omega 0|J\Omega\rangle^2}{C} \times \int_0^{E^*-E_L} 2T_f(E, L, \Omega)\rho(\Omega, E^* - E - E_L)dE, \tag{12}$$

where a normalization coefficient is used,

$$C = \sum_{L=0}^{L_M}\sum_{\Omega}\langle JL\Omega 0|J\Omega\rangle^2, \tag{13}$$

and the condition $J = L + \Omega$ is imposed. Here ρ represents the density of states, E_L is the the rotation energy in the fundamental state of the compound nucleus with an angular momentum L, and L_M is the maximum orbital momentum taken into consideration. This formula can be obtained easily by simplifying the model underlined in Ref. [2], that is, neglecting the additional collective excitations as γ, sloshing, or bending vibrations. Analog formulas can be obtained for the γ and neutron energy widths as detailed in Ref. [2].

In the fission channel, the spin Ω density of states can be shared as a function of the excitation energy between a discrete component and a continuum one:

$$\rho(J, E) = \begin{cases} \sum_i \delta(E - \epsilon_{\Omega,i}), & E < E_0 \\ \rho_{GC}(\Omega, E), & E \geqslant E_0 \end{cases}, \qquad (14)$$

where ρ_{CG} is the statistical Gilbert and Cameron approximation and $\epsilon_{\Omega,i}$ $(i = 1, n)$ are the set of diabatic single particle energies that are taken into consideration for a spin projection Ω. So that, the transmission in the fission channel can be decomposed as follows:

$$\int_0^{E^*-E_L} T_f(E, L, \Omega)\rho(\Omega, E^* - E - E_L)dE = \sum_i T_f(E^* - E_L - \epsilon_{\Omega,i}) + \int_0^{E^*-E_L-E_0} \times T_f(E, L, \Omega)\rho(\Omega, E^* - E - E_L)dE. \qquad (15)$$

The sum over i takes into account all the transmissions for diabatic levels with spin $J = \Omega + L$ located in the energy interval $[0, E_0]$. The transmission $T_f(E^* - E_L - \epsilon_{\Omega,i})$ means a weighted sum of the transmissions of all available diabatic energy paths emerging from the level $\epsilon_{\Omega,i}$.

The microscopic model used to compute the theoretical barrier is subject to some limitations as described in Ref. [22]. It is not possible to obtain pertinent values of the heights of the barriers. In these circumstances, it is necessary to use a phenomenological barrier. A phenomenological barrier is conventionally simulated as a function of a dimensionless parameter β, which characterizes a deformation, within three smoothed joined parabolas [38]. In our work, an imaginary component of the potential is added between the turning points of the second well, to simulate the damping due to γ and neutron emission. The values of this imaginary component are evaluated theoretically [2]. The additional excitations are considered as specialization energies and are added to the phenomenological barrier. This operation is achieved in the simplest possible way, by realizing a linear interpolation based on a correspondence between the elongation R and the dimensionless parameter β in some points. The correspondence was chosen for the two minimums, the two heights, and the exit point. The hybrid model emerges. New barriers are constructed as displayed in Fig. 9. When only the collective rotations are taken into account, the heights of the barriers and that of the second well are modified with the quantity

$$\Delta E_L = \frac{L(L + 2\Omega + 1)\hbar^2}{2I_j} - E_L, \qquad (16)$$

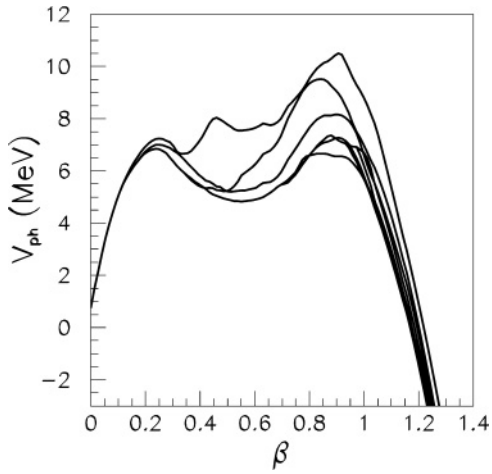

FIG. 9. The $\Omega = 1/2$ phenomenological V_{ph} barriers with excitations obtained in the frame of the hybrid model emerging from the fundamental level E_1.

where I_j is the moment of inertia and j labels one of the two heights or the second well. The decoupling parameter is neglected. The moment of inertia is computed simply with the formula $I_j = \mu R_j^2$, where μ is the reduced mass and R_j is the theoretical elongation obtained at the extreme point j. The quantity

$$E_L = \frac{L(L + 2\Omega + 1)\hbar^2}{2I_0} \qquad (17)$$

addresses the fundamental state of the compound nucleus. The previous formulas represent an improvement of the formalism found in Ref. [2].

A large number of excited states are obtained that are characterized by the projection Ω and the angular momentum L. The transmission is calculated numerically by approximating the shape of the excited barrier within 500 constant potential steps using the numerical recipe found in Ref. [39]. A search of the heights and of the widths of the phenomenological barrier is realized to reproduce as well as possible the experimental fission cross-section threshold structure. A behavior that agrees satisfactorily with the experimental data is obtained. The heights of the inner phenomenological barrier, the second well, and the outer barrier are 6.81, 4.83, and 6.61 MeV, respectively. In the same order, the widths are 1.2, 0.4, and 1.1 MeV. The theoretical cross-section is represented in Fig. 10 and compared with experimental data and evaluations.

The evaluations succeed in better reproducing the experimental data. In general many parameters are taken into account to evaluate a cross-section in terms of Bohr channels. For example, in evaluations phenomenological level density functions appropriately matched to the available experimental structure data at low excitation energies are used. Multiplication factors are also applied to level density functions to account for enhancements in the fission transition state densities at each fission barrier. It is a common practice to describe the cross-section as the sum of excitations for discrete levels constructed to fit the resonance. In other words, the evaluation takes into account many other parameters to fit the experimental data apart from the heights and the widths of

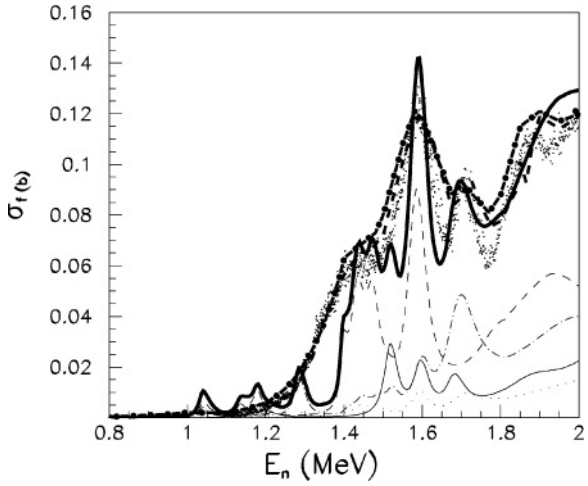

FIG. 10. The thick full line represents neutron-induced cross section for ^{232}Th as a function of the neutron incident energy E_n calculated within the hybrid model. Points are experimental data. The thick dashed line represents the ENDF/B-IV evaluation while the thick dot-dashed line is the JENDL-3.3 one [40]. Experimental data are from Refs. [5,6,41]. A thin full line gives the partial cross-section of spin 1/2, a dashed line is for the spin 3/2, the dot-dashed line is for 5/2, and the dotted line is for 7/2.

the phenomenological barrier. In the work presented in this article, no adjustments are made to improve the agreement, the simulations being based only on the phenomenological barrier parameters and the internuclear velocity.

Our simulations evidence an oscillatory behavior of the cross-section close to 1.4 MeV. This aspect is in agreement with the experimental data given in Ref. [42]. The experimental data combined with theoretical arguments estimate a ratio 2:1 between the partial cross-section of spin 3/2 and 1/2, respectively. The model shows that the partial cross-section for the spin 3/2 is responsible for the oscillations of the cross-section at these energies. Experimentally, the peak at 1.6 MeV is explained entirely by a partial cross-section of spin 3/2 with a small 5/2 component. In our plot a strong 3/2 component is present with small admixture of 1/2 and 5/2 partial cross-sections. A discrepancy is obtained for the 1.7 MeV structure. The experiment evidences the existence of a mixing between 3/2 and 5/2 components while our model predicts a large 5/2 partial cross-section followed by the 3/2 and 1/2 components.

In Fig. 11 the cross-section is plotted on an extended scale. It can be observed that the theoretical results exhibit an oscillatory behavior in the low energy region, up to 1.2 MeV, around the smooth variation of the experimental data. In Fig. 11(b), the transmissions computed for the barriers with different calculated excitations are displayed. The oscillatory behavior is due to the large number of resonances associated with the different excited barriers.

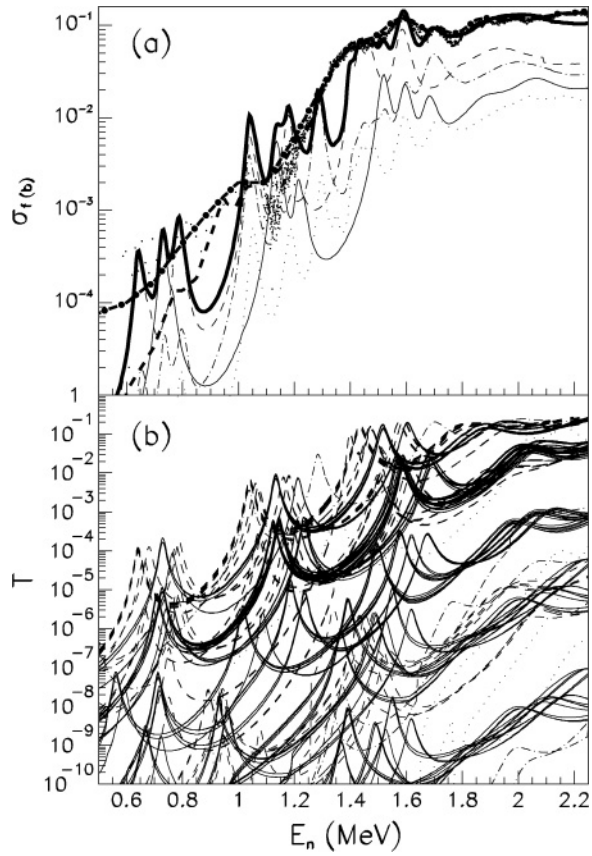

FIG. 11. (a) Same as Fig. 10 in an extended logarithmic scale along the y axis. (b) $L = 0$ fission transmissions for different barriers as a function of the neutron energy E_n. The transmissions for $\Omega = 1/2$ excitations are plotted with full lines, those for 3/2 with a dashed line, those for 5/2 with a dot-dashed line, and those for 5/2 with a dotted line.

IV. SUMMARY AND DISCUSSION

The scope of the present work is to investigate the mechanism for the formation of the fission cross-section structure and to understand the formation of a huge number of resonances by appealing essentially to dynamical single-particle effects associated with β vibration in the second well. The number of free parameters is kept as minimal as possible (six parameters that characterize the phenomenological barrier and one parameter for the internuclear velocity) to show evidence of the physics of the problem.

Theoretical excitations and their associated probabilities were determined for a given partition in the isotopic distribution of fragments. These excitations were added to a phenomenological barrier in the framework of the hybrid model. After a suitable search of the parameters of the double-humped phenomenological barrier, the cross-section was computed. The results give a rather good qualitative agreement with experimental data. It is evidenced that the structure at 1.4 and 1.6 MeV is mainly dominated by spin 3/2 partial cross-section with a small admixture of spin 1/2, while the structure at 1.7 MeV is given by a large partial cross-section of spin 5/2.

In this exploratory analysis, only one partition for the fission fragments is taken into consideration. For other partitions in the same mass region, it is expected that the level scheme changes slightly leading to a small shift in the energy of the resonances. By taking into account several partitions in the

same mass region and folding their yields it it possible to obtain broader resonances as experimentally observed.

In this context, it will be interesting to explore experimentally if the isotopic fragment distribution in the fission process changes in the energy region covered by a resonance, showing a preference for only several mass partitions. If such a phenomenon can be experimentally evidenced, that will represent a strong experimental support for our model because the statistical theories don't include ingredients related to this aspect.

The model can be further improved. Up to now, only the radial coupling was used to explain the intermediate structure of the cross-section. It is possible to have better results by taking into account the Coriolis mixing and the residual interactions by using evolved forms for the system of coupled equations that describes the microscopic motion [33,43].

Other models succeed in better reproducing the experimental data [44] using an extensive number of free parameters: 10 variables for the heights and widths of the triple-humped phenomenological barrier plus 5 times 16 variables for the transition bandheads constructed on different intrinsic excitations (with a significance of excitations given by single-particle energies). Despite the overall excellent agreement on a very large neutron energy region, this treatment, generally used in evaluations, takes into account a peculiar behavior for the single-particle excitation energies. The levels that characterize the transition bandheads never intersect. The first $\frac{1}{2}^+$ level have practically the same value (having as reference the fundamental state) during the penetration of the barrier. This behavior, as remarked previously, cannot be expected. These transition levels are introduced to fit resonances. Moreover, the statistical models consider that the population of each fundamental transition band is essentially one. The formalism presented in the Sec. II indicates that such a behavior is physically not reasonable.

The possibility to jump from one level to another was predicted by Hill and Wheeler in Ref. [45]. Dissipation in terms of Landau-Zener crossings during fission was first proposed in Ref. [46] where excitations were considered only for time-reversed pairs, neglecting the possible existence of unpaired nucleons. Since then, many studies have been performed, but it was the first time that the Landau-Zener effect was used to investigate the resonant structure of the fission cross-section.

The dissipation energy during the fission process was computed using Rel. (9) keeping the same internuclear velocity as in the case of single-particle occupation probabilities. The results are plotted in Fig. 12 for three different channels, that is, paths 1, 7, and 22 given in Table I. For each diabatic path, due to the blocking effect, the system (8) is solved without the level occupied by the unpaired nucleon. Up to the second barrier, the nucleus is cold, the dissipated energy being very low. Penetrating the second barrier, the dissipated energy increases. In the region of the second well, the dissipated energies for

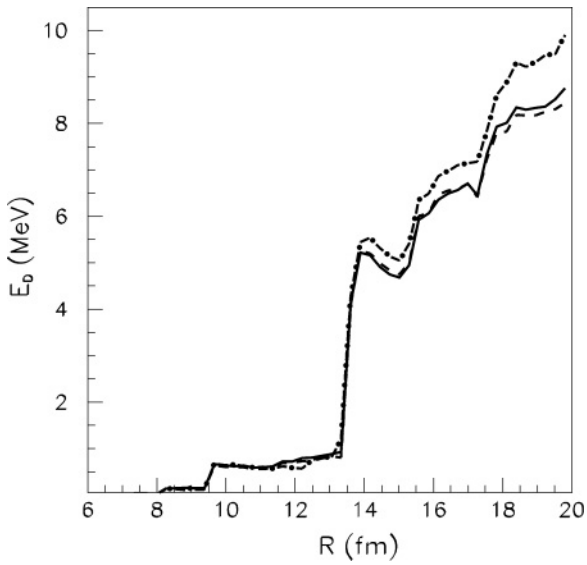

FIG. 12. Dissipated energies during the fission process for three energy paths: full line for trajectory No. 1, dashed line for trajectory No. 7, and dot-dashed line for trajectory No. 20 of Table I.

the three channels fall in a 0.3 MeV interval. The height of the second minimum has a crucial influence on the position of the resonances. Therefore, if the dissipated energy is taken into account, some shifts of the positions of the resonances can be expected. This problem was neglected in all analyses of fission cross-section resonant structure.

The present investigation shows that the resonant structure of the fission cross-section can be explained by the existence of many barriers associated with single-particle excitations. So, it is possible that the complex structure in the fission cross-section is due to rearrangement of orbitals and the dynamic of the process, beginning from the initial state of the compound nucleus and terminating at the scission. A large number of different excited barriers are formed leading to a large number of vibrational resonances in the second well. These resonances carry information about the structure of the nucleus at hyperdeformations and the dynamics. The model presented in this work represents an alternative to the actual statistical models and may determine a competitive way to consider the fission process. New information on the basic mechanisms of nuclear fission can be obtained by mixing accurate experimental data with new theories that take into account the nuclear structure of the nuclear system during the whole disintegration process. The new experimental values concerning the ^{234}U(n,f) cross-section [47], obtained in the n-TOF program, displayed a structure of suprabarrier resonances that are not of statistical nature. Phenomenological and statistical models based on the saddle density of states cannot explain this rich resonant structure up to 20 MeV energies. However, new methods are required.

[1] N. Bohr and J. Wheeler, Phys. Rev. **16**, 426 (1939).
[2] M. Mirea, L. Tassan-Got, C. Stephan, C. O. Bacri, P. Stoica, and R. C. Bobulescu, J. Phys. G **31**, 1165 (2005).
[3] M. Mirea and R. K. Gupta, in *Heavy Elements and Related New Phenomena*, edited by W. Greiner and R. J. Gupta (World Scientific, Singapore, 1999), Vol. 2, p. 765.

[4] G. D. James, J. E. Lynn, and L. G. Earwaker, Nucl. Phys. **A189**, 225 (1972).
[5] J. Blons, C. Mazur, D. Paya, M. Ribrag, and H. Weigmann, Phys. Rev. Lett. **41**, 1282 (1978).
[6] J. Blons, C. Mazur, and D. Paya, Phys. Rev. Lett. **35**, 1749 (1975).
[7] P. Moller, Nucl. Phys. **A192**, 529 (1972).
[8] J. Blons, C. Mazur, D. Paya, M. Ribrag, and H. Weigmann, Nucl. Phys. **A414**, 1 (1984).
[9] J. Caruana, J. W. Boldemann, and R. L. Walsh, Nucl. Phys. **A285**, 205 (1977).
[10] J. W. Boldeman, D. Cogny, A. R. de L. Musgrove, and R. L. Walsh, Phys. Rev. C **22**, 627 (1980).
[11] M. Mirea, L. Tassan-Got, C. Stephan, C. O. Bacri, and R. C. Bobulescu, Europhys. Lett. **73**, 705 (2006).
[12] U. Brosa, S. Grossman, and A. Muller, Phys. Rep. **197**, 167 (1990).
[13] J. A. Wheeler, *Niels Bohr and the Development of Physics*, edited by W. Pauli, L. Rosenfeld, and W. Weisskopf (Pergamon, London, 1955), p. 163.
[14] T. Ledergerber and H.-C. Pauli, Nucl. Phys. **A207**, 1 (1973).
[15] J. P. Bocquet and R. Brissot, Nucl. Phys. **A502**, 213c (1989).
[16] J. F. Berger, M. Girod, and D. Gogny, Nucl. Phys. **A428**, 23c (1984).
[17] P. Moller and A. Iwamoto, Phys. Rev. C **61**, 047602 (2000).
[18] M. Mirea, L. Tassan-Got, C. Stephan, and C. O. Bacri, Nucl. Phys. **A735**, 21 (2004).
[19] D. N. Poenaru, M. Ivascu, and D. Mazilu, Comput. Phys. Commun. **19**, 205 (1980).
[20] M. Brack, J. Damgaard, A. Jensen, H. Pauli, V. Strutinsky, and W. Wong, Rev. Mod. Phys. **44**, 320 (1972).
[21] M. Mirea, Phys. Rev. C **54**, 302 (1996).
[22] M. Mirea, Nucl. Phys. **A780**, 13 (2006).
[23] K. T. R. Davies, A. J. Sierk, and J. R. Nix, Phys. Rev. C **13**, 2385 (1976).
[24] R. Capote, S. Goriely, S. Hilaire, A. Konnig, and M. Sin, in *International Conference for Nuclear data and Technology (ND2007), April 22–27 2007, Nice, France* (in print).
[25] R. Smolanczuk, J. Skalski, and A. Sobiczewski, Phys. Rev. C **52**, 1871 (1995).
[26] Z. Patyk, J. Skalski, A. Sobiczewsky, and S. Cwiok, Nucl. Phys. **A502**, 591c (1989).
[27] S. G. Nilsson, C. F. Tsang, A. Sobiczewski, Z. Szymansky, S. Wicech, C. Gustafson, I.-L. Lamm, P. Moler, and B. Nilsson, Nucl. Phys. **A131**, 1 (1969).
[28] A. Thiel, J. Phys. G **16**, 867 (1990).
[29] J. Y. Park, W. Greiner, and W. Scheid, Phys. Rev. C **21**, 958 (1980).
[30] A. Diaz-Torres and W. Scheid, Nucl. Phys. **A757**, 373 (2005).
[31] A. Diaz-Torres, Phys. Rev. C **74**, 064601 (2006).
[32] M. Mirea, Phys. Rev. C **57**, 2484 (1998).
[33] M. Mirea, Phys. Rev. C **63**, 034603 (2001).
[34] W. Greiner, J. Y. Park, and W. Scheid, *Nuclear Molecules* (World Scientific, Singapore, 1995), Chap. 11.
[35] S. E. Koonin and J. R. Nix, Phys. Rev. C **13**, 209 (1976).
[36] J. Blocki and H. Flocard, Nucl. Phys. **A273**, 45 (1976).
[37] R. G. Moore, Rev. Mod. Phys. **32**, 101 (1960).
[38] J. D. Cramer and J. R. Nix, Phys. Rev. C **2**, 1048 (1970).
[39] S. Bjornholm and J. E. Lynn, Rev. Mod. Phys. **52**, 752 (1980).
[40] http://www.nndc.bnl.gov/index.jsp.
[41] O. Shcherbakov, A. Donets, A. Evdokimov, A. Fomichev, T. Fukahori, A. Hasegawa, A. Laptev, V. Maslov, G. Petrov, S. Soloviev, Y. Tuboltsev, and A. Vorobyev, J. Nucl. Sci. Technol. Suppl. **2**, 230 (2002).
[42] G. F. Auchampaugh, S. Plattard, N. W. Hill, G. de Saussure, R. B. Perez, and J. A. Harvey, Phys. Rev. C **24**, 503 (1981).
[43] M. Mirea, Mod. Phys. Lett. **A18**, 1809 (2003).
[44] M. Sin, R. Capote, A. Ventura, M. Herman, and P. Oblozinsky, Phys. Rev. C **74**, 014608 (2006).
[45] D. L. Hill and J. A. Wheeler, Phys. Rev. **89**, 1102 (1953).
[46] G. Schutte and L. Wilets, Z. Phys. A **286**, 313 (1978).
[47] C. P. Dobarro, Ph.D. thesis, *Measurements of the U-234(n,f) Cross Section with PPAC Detectors at the n_TOF Facility*, Universidad de Santiago de Compostela, June 2005.